

Energy transfer mechanisms and resolvent analysis in the cylinder wake

Bo Jin[†], Sean Symon, and Simon J. Illingworth

Department of Mechanical Engineering, University of Melbourne, VIC, 3010, Australia

(Received xx; revised xx; accepted xx)

Energy transfer mechanisms for vortex shedding behind a 2D cylinder at a Reynolds number of $Re = 100$ are investigated. We first characterize the energy balances achieved by the true cylinder flow—both for the flow as a whole and for each of its most energetic harmonic frequencies. It is found that viscous dissipation balances production when each is considered over the entire flow field and therefore that linear mechanisms achieve an energy balance on their own, thus respecting the Reynolds–Orr equation. Nevertheless, nonlinear energy transfer plays a critical role in the transfer of energy across temporal frequencies. Suitable energy conservation laws reveal that while nonlinear energy transfer mechanisms neither produce nor consume energy overall, they nevertheless account for an important transfer of energy between temporal frequencies. We then compare the energy balance for DNS to that predicted by resolvent analysis. Although a suitable energy balance is achieved for each harmonic, resolvent analysis does not respect the conservative nature of the nonlinear terms and fails to model nonlinear energy transfer between temporal frequencies. This lack of nonlinear energy transfer helps to explain the excess energy of the leading resolvent mode observed in the far wake.

Key words: ...

1. Introduction

Shear flows occur whenever a fluid flows past a solid object and are therefore commonplace in engineering and in nature. Despite being governed by the Navier–Stokes equations—a set of nonlinear partial differential equations—certain important aspects of shear flows are well described by linear mechanisms (Schmid & Henningson 2001). This is true not only for small perturbations away from some laminar base flow, but also for fully developed turbulent shear flows for which the fluctuations are not small. For fully developed turbulent shear flows, a linear operator can be formed about the time-averaged mean flow and the remaining nonlinear terms are then treated as a forcing to an otherwise linear system (Landahl 1967; Bark 1975). In this way no linearization is performed. Rather one characterizes the response of the linear operator to the remaining nonlinear terms. In this context resolvent analysis—in which the linear operator is characterized in the frequency domain by forming its temporal frequency response (its resolvent)—has been used with particular success in recent years (McKeon & Sharma 2010). Despite its success, some of the predictions of resolvent analysis show important discrepancies with the true flow. Of particular note for the present work is that *i*) the predictions of resolvent analysis are often improved by including an eddy viscosity in the linear operator (Hwang

[†] Email address for correspondence: bjin1@student.unimelb.edu.au

& Cossu 2010; Mettot *et al.* 2014; Illingworth *et al.* 2018); and that *ii*) for some shear flows such as the cylinder wake (Rosenberg *et al.* 2019) and the flow past an airfoil (Yeh & Taira 2019; Symon *et al.* 2019), the leading resolvent response mode is too energetic in the far wake.

This work considers resolvent analysis and energy transfer mechanisms for the two-dimensional flow past a cylinder at a Reynolds number of 100. The work is in two parts. First, by performing an harmonic decomposition of the cylinder wake we characterize, for each harmonic mode, the linear and nonlinear energy transfer mechanisms for the true cylinder flow. Second, the true energy transfer is compared to that predicted by a resolvent analysis of each harmonic mode. By doing so we will uncover two things. First, we characterize—both for the true flow and for resolvent analysis—the energy balance between production, dissipation and nonlinear transfer for each harmonic mode. Second, we show that, although resolvent analysis achieves a suitable energy balance for any single harmonic mode, it does not achieve the correct energy balance across modes. In particular we will observe a significant nonlinear transfer of energy from the first harmonic mode to the second and third harmonic modes in DNS. We will see that this energy transfer is not captured by resolvent analysis, which helps to explain the excess energy of the leading resolvent mode in the far wake (Yeh & Taira 2019; Symon *et al.* 2019).

2. Problem formulation

The incompressible Navier-Stokes equations describe the conservation of mass and momentum of an incompressible fluid:

$$\begin{aligned}\partial_t \mathbf{u} &= -\mathbf{u} \cdot \nabla \mathbf{u} - \nabla p + Re^{-1} \nabla^2 \mathbf{u}, \\ \nabla \cdot \mathbf{u} &= 0.\end{aligned}\tag{2.1}$$

The equations have been nondimensionalized by the free-stream velocity U_∞ and the cylinder diameter D . The Reynolds number is therefore defined as $Re = U_\infty D / \nu$, where ν is the kinematic viscosity. For a fully developed flow, an evolution equation can be derived for the fluctuations (\mathbf{u}', p') by forming a linear operator about the mean (time-averaged) flow (\mathbf{U}, P) and treating the remaining nonlinear terms as an exogenous forcing (Landahl 1967; Bark 1975; McKeon & Sharma 2010):

$$\begin{aligned}\partial_t \mathbf{u}' &= L \mathbf{u}' - \nabla p' + \mathbf{f}', \\ \nabla \cdot \mathbf{u}' &= 0.\end{aligned}\tag{2.2}$$

Thus the fluctuations evolve according to the linear operator $L = -\mathbf{U} \cdot \nabla() - () \cdot \nabla \mathbf{U} + Re^{-1} \nabla^2()$ and the forcing they receive from the remaining nonlinear terms $\mathbf{f}' = -\mathbf{u}' \cdot \nabla \mathbf{u}' + \overline{\mathbf{u}' \cdot \nabla \mathbf{u}'}$. (Here $\overline{(\cdot)}$ denotes a time average.) Note that the pressure term in (2.2) could be eliminated by projecting the velocity field onto the space of divergence-free functions, but we choose to retain pressure for the moment because its influence will be eliminated naturally when we consider the flow's energy balance in §3.

2.1. Linear input/output (resolvent) analysis

Resolvent analysis proceeds by taking Laplace transforms of (2.2), setting $s = j\omega$ and rearranging to arrive at the frequency response (or resolvent):

$$\mathcal{H}(\omega) = \mathbf{P}^T \left(j\omega \mathbf{I} + \begin{bmatrix} -L & \nabla() \\ \nabla \cdot () & 0 \end{bmatrix} \right)^{-1} \mathbf{P}\tag{2.3}$$

so that, at frequency ω ,

$$\hat{\mathbf{u}}(\omega) = \mathcal{H}(\omega)\hat{\mathbf{f}}(\omega). \quad (2.4)$$

Here \mathbf{P} is the prolongation matrix that maps a velocity vector $\hat{\mathbf{u}}$ to a velocity-zero-pressure vector $[\hat{\mathbf{u}}, 0]$. Rather than consider the exact form of the nonlinear forcing $\hat{\mathbf{f}}$, resolvent analysis instead considers the optimal forcing that achieves the maximum energetic gain $\gamma^2(\omega)$ at each frequency. This analysis gives important information on the system's linear dynamics by characterizing its global frequency response to external forcing (Sipp & Marquet 2013). The linear optimization to be performed is

$$\gamma^2(\omega) = \max_{\hat{\mathbf{f}}} \frac{\langle \hat{\mathbf{u}}^*, \hat{\mathbf{u}} \rangle}{\langle \hat{\mathbf{f}}^*, \hat{\mathbf{f}} \rangle} = \max_{\hat{\mathbf{f}}} \frac{\langle \hat{\mathbf{f}}^* \mathcal{H}^*(\omega), \mathcal{H}(\omega) \hat{\mathbf{f}} \rangle}{\langle \hat{\mathbf{f}}^*, \hat{\mathbf{f}} \rangle} = \sigma_1^2(\mathcal{H}(\omega)), \quad (2.5)$$

where $\langle \cdot, \cdot \rangle$ denotes the inner product over the spatial domain Ω . This optimization problem can be solved by performing a singular value decomposition of the resolvent operator $\mathcal{H}(\omega)$: that is, the leading singular value squared, $\sigma_1^2(\mathcal{H}(\omega))$, corresponds to the maximum energy gain $\gamma^2(\omega)$ at frequency ω , as expressed by (2.5).

2.2. Flow configuration and discretization

We consider the incompressible flow past a two-dimensional circular cylinder at a Reynolds number of $Re = 100$. Both the direct numerical simulations (DNS) and the linear analyses have been performed using FEniCS (Logg *et al.* 2012) using the same mesh, boundary conditions and discretization as those described in Jin *et al.* (2019).

We simulate the full nonlinear equations (2.1) using a time step $\Delta t = 0.01$. A second-order implicit scheme is used for time discretization and the resulting nonlinear equations are solved directly using a Newton method. The simulations give rise to vortex shedding at a Strouhal number of $St = 0.1677$. This is consistent with the results of Jiang & Cheng (2017) and corresponds to a fundamental frequency of $\omega_1 = 1.054$. The time-averaged mean flow is then obtained by time-averaging over 54 periods after the flow has settled to saturated vortex shedding, and the fluctuations are extracted for Fourier analysis. The corresponding energy spectrum is shown in figure 1(a), which displays sharp peaks at the fundamental frequency ω_1 (marked by a red dashed line) and its higher harmonics $\omega_n = n\omega_1$. It is important to note that more than 99.9% of the total fluctuation energy is concentrated in the first three harmonic frequencies ω_1 , ω_2 and ω_3 .

We also characterize in figure 1(b) the linear resolvent operator (2.3) of the fully developed cylinder wake by plotting its maximum energy gain (2.5) for a range of temporal frequencies ω . We observe a single resonant peak (marked by a blue dashed line) at $\omega_r = 1.04$, as reported in Symon *et al.* (2018). Finally, we further characterize both the DNS and resolvent operator (2.3) by plotting *i*) the spatial distribution of the kinetic energy of the first harmonic mode from DNS in figure 1(c); and *ii*) the spatial distribution of the kinetic energy of the leading resolvent response mode at frequency ω_1 in figure 1(d). Although there is reasonable agreement between the two kinetic energy distributions in panels (c) and (d), we do also observe some differences. Perhaps the most obvious is that the kinetic energy of the leading resolvent response mode in (d) is too energetic in the far wake when compared to the first harmonic mode from DNS in (c).

2.3. Harmonic decomposition

Motivated by the results of figure 1(a)—where we observed that the energy of the DNS velocity field is concentrated in a small number of discrete frequencies—we now

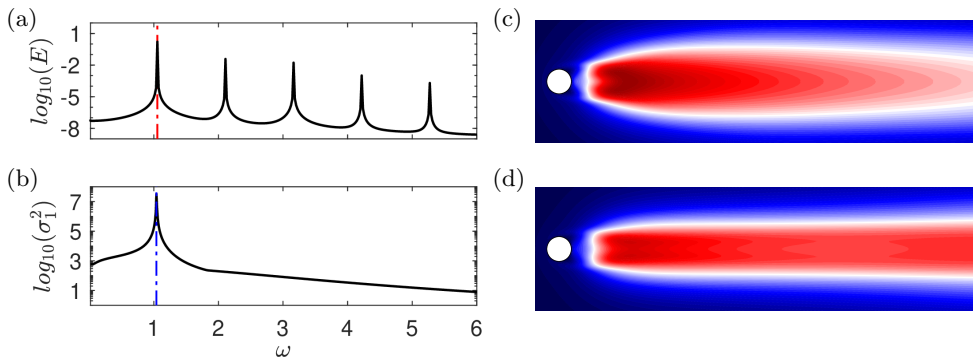


FIGURE 1. (a) Energy spectrum of perturbation velocity from DNS. (b) Leading energy gains σ_1^2 from resolvent analysis. Spatial distribution of the kinetic energy for (c) 1st harmonic mode from DNS and (d) optimal response at 1st harmonic frequency from resolvent analysis. Both contour plots share the same color scale.

posit an harmonic decomposition of the fluctuating velocity field \mathbf{u}' :

$$\mathbf{u}' = \sum_n \hat{\mathbf{u}}^{(n)} e^{j\omega_n t} + \text{c.c.}, \quad (2.6)$$

and similarly for p' and \mathbf{f}' , where (c.c.) denotes the complex conjugate. This decomposition will be of particular significance when we consider the physical mechanisms by which energy is exchanged across temporal frequencies. We again note that more than 99.9% of the total fluctuation kinetic energy is contained in the first three harmonic frequencies (see §2.2 and figure 1(a)).

3. Energy transfer framework

In this section we consider the energy balance achieved *i*) by the cylinder flow overall; and *ii*) by each harmonic mode $\hat{\mathbf{u}}^{(n)}$ in the harmonic decomposition (2.6).

3.1. Energy balance for the flow overall

We can form an evolution equation for the total kinetic energy of the fluctuations by taking the kinetic-energy inner product of the perturbation equations (2.2) with \mathbf{u}' :

$$\langle \mathbf{u}', \partial_t \mathbf{u}' \rangle = \langle \mathbf{u}', L\mathbf{u}' - \nabla p' \rangle + \langle \mathbf{u}', \mathbf{f}' \rangle. \quad (3.1)$$

Expanding each term in (3.1) using tensor notation and averaging in time we arrive at

$$\begin{aligned} \frac{d\bar{E}}{dt} &= \underbrace{\int -\overline{u'_i u'_j} \frac{\partial U_i}{\partial x_j} d\Omega}_P + \underbrace{Re^{-1} \int -\frac{\partial u'_i}{\partial x_j} \frac{\partial u'_i}{\partial x_j} d\Omega}_D \\ &+ \underbrace{\int \left(-\frac{1}{2} \overline{u'_i u'_i U_j}\right) \cdot n_j d\Gamma_{\text{out}}}_M + \underbrace{\int \left(-\frac{1}{2} \overline{u'_i u'_i u'_j}\right) \cdot n_j d\Gamma_{\text{out}}}_N, \end{aligned} \quad (3.2)$$

Equation (3.2) is the Reynolds-Orr equation with additional terms M and N to account for any fluxes of energy out of the domain Ω . These additional terms appear as line integrals across the domain's outlet Γ_{out} after using Gauss' theorem, the boundary

conditions, and the divergence-free condition of (2.2). Note that the pressure field has been eliminated due to the zero-stress boundary condition at the outlet, $(-u'_i p' \delta_{ij} + Re^{-1} u'_i \partial u'_i / \partial x_j) \cdot n_j = 0$, where n_j denotes the outward-pointing normal vector on the boundary. If vortex shedding is fully developed then $d\bar{E}/dt = 0$ and it follows that the four terms in (3.2) must balance so that their sum is zero.

The four terms in (3.2) represent energy production (P); viscous dissipation (D); energy flux out by the mean flow (M); and work done by the nonlinear terms (N). (The work done by the nonlinear terms, N , can also be interpreted as the flux of energy out of the domain by the fluctuations.) In general we expect production P , which represents the energy extracted from the mean flow by the fluctuations, to be positive. Viscous dissipation D , meanwhile, is always negative. The energy flux terms M and N represent the energy leaving the domain by linear (M) or nonlinear (N) mechanisms. Note that both M and N tend to zero if the outlet boundary is placed infinitely far from the cylinder since any fluctuations will dissipate before reaching the boundary. In this case (3.2) simplifies to the Reynolds–Orr equation which states that, when considered over the entire domain, dissipation balances production.

3.2. Energy balance for each harmonic mode

We can derive a similar energy balance for each harmonic mode by substituting the harmonic decomposition (2.6) into (2.2) and (after using the orthogonality of the complex exponentials) taking the inner product with $\hat{\mathbf{u}}^*$:

$$\langle \hat{\mathbf{u}}^*, j\omega \hat{\mathbf{u}} \rangle + \text{c.c.} = \langle \hat{\mathbf{u}}^*, L\hat{\mathbf{u}} - \nabla \hat{p} \rangle + \text{c.c.} + \langle \hat{\mathbf{u}}^*, \hat{\mathbf{f}} \rangle + \text{c.c.} \quad (3.3)$$

(For simplicity the superscript on $\hat{\mathbf{u}}$ in (2.6) has been removed.) Expanding (3.3) and again using tensor notation we arrive at

$$\begin{aligned} j\omega \hat{E} + \text{c.c.} = & \underbrace{\int -(\hat{u}_i^* \hat{u}_j + \hat{u}_i \hat{u}_j^*) \frac{\partial U_i}{\partial x_j} d\Omega}_{\hat{P}(\omega)} + \underbrace{\frac{2}{Re} \int -\frac{\partial \hat{u}_i^*}{\partial x_j} \frac{\partial \hat{u}_i}{\partial x_j} d\Omega}_{\hat{D}(\omega)} \\ & + \underbrace{\int (-\hat{u}_i^* \hat{u}_i U_j) \cdot n_j d\Gamma_{\text{out}}}_{\hat{M}(\omega)} + \underbrace{\int (\hat{u}_i^* \hat{f}_i + \hat{u}_i \hat{f}_i^*) d\Omega}_{\hat{N}(\omega)}. \end{aligned} \quad (3.4)$$

The left-hand side of (3.4) satisfies $j\omega \hat{E} + \text{c.c.} = 0$ for fully developed vortex shedding, indicating that each harmonic mode neither gains nor loses energy over one cycle. Therefore similar to the global energy balance (3.2), there also exists a balance for each harmonic mode across the four terms $\hat{P}(\omega)$, $\hat{D}(\omega)$, $\hat{M}(\omega)$ and $\hat{N}(\omega)$. Note that, due to the summation over complex conjugate pairs, all terms in (3.4) are real-valued.

The forcing $\hat{\mathbf{f}}$ in (3.4) could either represent the true nonlinear forcing from DNS or be replaced by the leading input resolvent mode given by (2.5). The term $\hat{N}(\omega_n)$ represents the work done by the nonlinear forcing on harmonic mode n and can be positive or negative. If $\hat{N}(\omega_n)$ is positive (negative) then the nonlinear terms give energy to (take energy from) harmonic mode n . It is important to note that, due to the unitary property of the Fourier transform, we may link the energy balance at each frequency ω_n to the energy balance for the flow overall. For production, for example:

$$P = \sum_n \hat{P}(\omega_n), \quad (3.5)$$

and similarly for D , M and N . (Note that this will hold only approximately due to the truncation to three modes of the harmonic decomposition (2.6).)

4. Energy transfer in the cylinder wake

We now compare the energy balance achieved across production, dissipation and nonlinear transfer for DNS and resolvent analysis. Specifically we will consider the energy balance *i*) for each harmonic mode; *ii*) for the flow as a whole; and *iii*) for the nonlinear transfer between modes. It will be convenient to define a linear dissipation term, $\hat{D}_e(\omega) = \hat{D}(\omega) + \hat{M}(\omega)$ for each harmonic mode and $D_e = D + M$ for the flow as a whole, to denote the total effective dissipation due to linear mechanisms. The energy balance across production, linear dissipation and nonlinear transfer for DNS and resolvent analysis is plotted in figures 2 and 3, which show the same information but in different ways. In figure 2 the energy balance is arranged by harmonic mode, each row representing a single harmonic. In figure 3 the energy balance is instead arranged by physical mechanism: the first row for production, P ; the second row for the total linear dissipation, D_e ; and the third row for nonlinear transfer, N . In both figures the energy balance is shown for DNS in panel (a) and for resolvent analysis in panel (b).

4.1. Energy balance for the DNS

Let us start with the DNS data. The first observation is that the vast majority of both production and dissipation is achieved by the first harmonic mode, ω_1 . We also note that, for each harmonic mode, there exists an energy balance between production $\hat{P}(\omega_n)$, dissipation $\hat{D}_e(\omega_n)$, and nonlinear transfer $\hat{N}(\omega_n)$:

$$\hat{P}(\omega_n) + \hat{D}_e(\omega_n) + \hat{N}(\omega_n) = 0. \quad (4.1)$$

This is most clearly seen in figure 2 (a). For the first harmonic mode, production exceeds dissipation ($\hat{P}(\omega_1) > \hat{D}_e(\omega_1)$) and the difference between them is balanced by a negative nonlinear transfer ($\hat{N}(\omega_1) < 0$). For the second and third harmonics the inverse is true: for both modes, dissipation exceeds production ($\hat{D}_e(\omega_2) > \hat{P}(\omega_2)$, $\hat{D}_e(\omega_3) > \hat{P}(\omega_3)$) and for each the difference between them is balanced by a positive nonlinear transfer ($\hat{N}(\omega_2) > 0$, $\hat{N}(\omega_3) > 0$). We also observe a similar balance between production, dissipation and nonlinear transfer across all modes in aggregate:

$$\sum_n (\hat{P}(\omega_n) + \hat{D}_e(\omega_n) + \hat{N}(\omega_n)) = 0. \quad (4.2)$$

This second balance follows naturally from the first by summing (4.1) over the three harmonic modes. It therefore follows that there exists a similar balance between production, dissipation and nonlinear transfer for the flow as a whole.

A third energy balance is achieved by the DNS: The nonlinear transfer terms satisfy

$$N = \sum_n \hat{N}(\omega_n) \approx 0. \quad (4.3)$$

This balance is most clearly seen in figure 3 (a). From (3.2) it implies that the energy flux out of the domain due to the nonlinear terms is negligible and therefore that the nonlinear transfer terms are conservative—that is, that they neither create nor destroy energy when integrated over the entire flow.

It is instructive now to consider the manner in which the nonlinear balance (4.3) is achieved in DNS. From figure 3 (a) we observe that the nonlinear transfer is negative for the first harmonic ($\hat{N}(\omega_1) < 0$) and positive for the higher harmonics ($\hat{N}(\omega_2) > 0$, $\hat{N}(\omega_3) > 0$). This implies that the first harmonic loses energy by nonlinear transfer, which is balanced by positive nonlinear transfer for the remaining harmonics. Together the nonlinear transfer terms therefore act as an inter-mode mediator, taking energy from

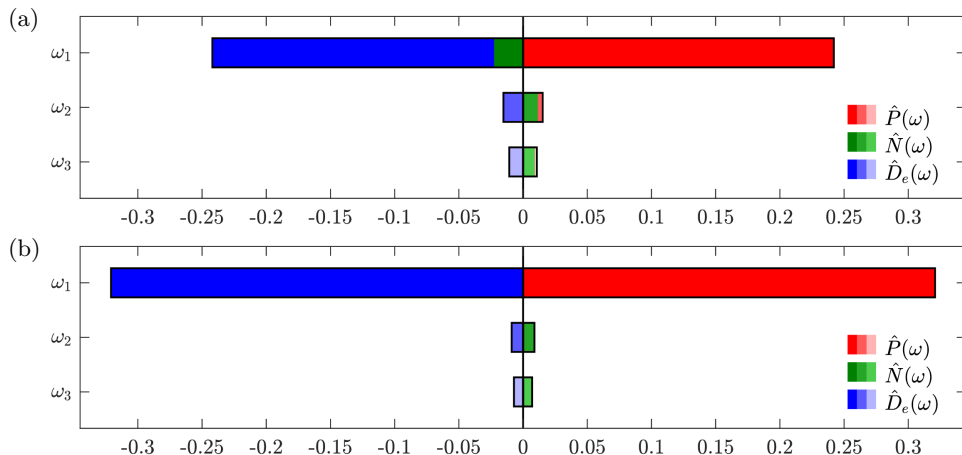


FIGURE 2. Harmonic energy balance at the first three harmonic frequencies for (a) DNS and (b) resolvent analysis across production, linear dissipation and nonlinear energy transfer, denoted as $\hat{P}(\omega)$, $\hat{D}_e(\omega)$ and $\hat{N}(\omega)$ respectively.

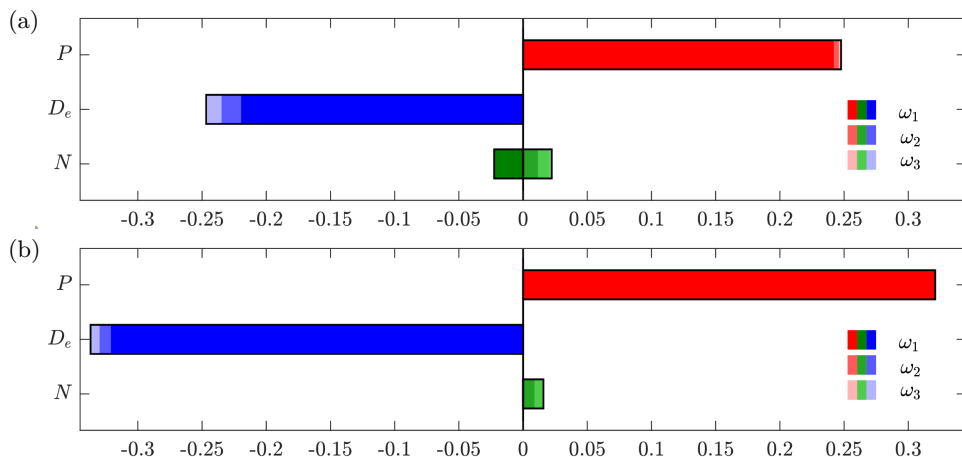


FIGURE 3. Energy balance for (a) DNS and (b) resolvent analysis (summing over the first three harmonic frequencies) across production, linear dissipation and nonlinear energy transfer, which are denoted as P , D_e and N , respectively.

modes that produce more energy than they dissipate and giving it to modes that dissipate more energy than they produce.

4.2. Energy balance for resolvent analysis

We now consider the extent to which the energy balances established in §4.1 for the DNS are respected by resolvent analysis. We stress here the assumption implicit in the resolvent analysis that each harmonic mode is forced by its leading resolvent forcing mode at its corresponding frequency ω_1 , ω_2 or ω_3 . We also note that, since resolvent analysis is linear, the amplitudes of the terms $\hat{P}(\omega_n)$, $\hat{D}_e(\omega_n)$ and $\hat{N}(\omega_n)$ are arbitrary. We have therefore selected mode amplitudes such that the total kinetic energy for resolvent analysis is the same as the total kinetic energy for the DNS.

We see in figure 2 (b) that, for each harmonic mode, the energy balance (4.1) is achieved by resolvent analysis. This balance ensures that each harmonic mode, as modelled by the

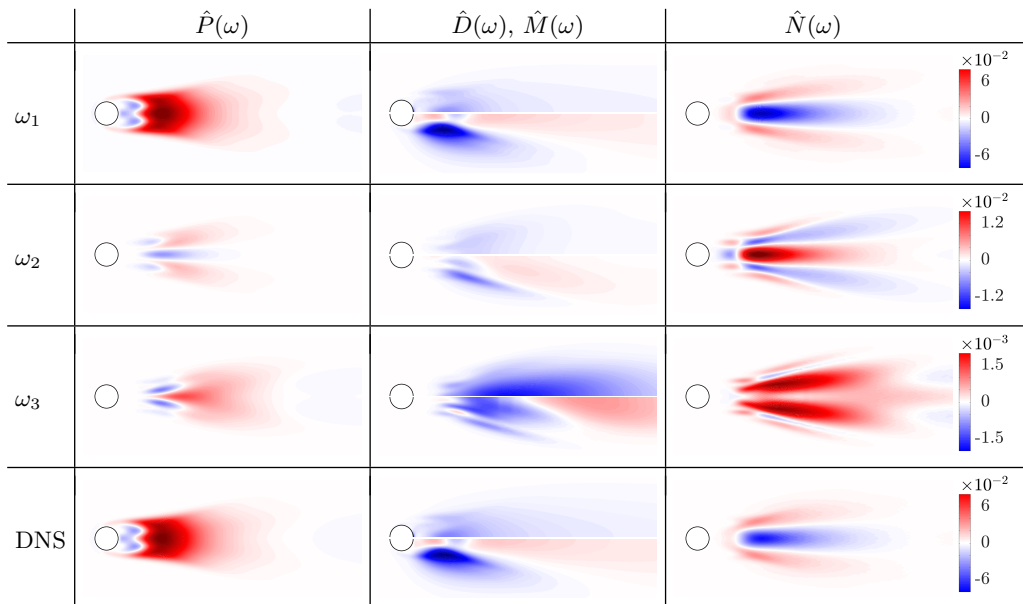


FIGURE 4. Spatial distribution of production ($\hat{P}(\omega)$), viscous dissipation ($\hat{D}(\omega)$, upper half) / energy flux out ($\hat{M}(\omega)$, lower half) and nonlinear energy transfer ($\hat{N}(\omega)$) from DNS for each harmonic frequency. Note the smaller colour scales for ω_2 and ω_3 .

resolvent, neither gains nor loses energy over a cycle. This balance for each harmonic mode in turn ensures that there also exists a similar balance over all modes, i.e. that the second balance (4.2) is also satisfied by resolvent analysis.

We come now to a key difference between the DNS and resolvent analysis: the energy balance for the nonlinear transfer terms $\hat{N}(\omega_n)$. In figure 3 (b) we observe that resolvent analysis, unlike the DNS, does not satisfy the nonlinear balance (4.3). The implication is that, when each harmonic mode is assumed to be forced by its leading forcing mode, the resulting energy transfers between these harmonics do not satisfy the constraints placed on them by the Navier–Stokes equations. We therefore observe that the conservative nature of the nonlinear forcing observed for the DNS, as expressed by (4.3), is not satisfied by the resolvent analysis.

4.3. Spatial distribution of the energy balance

Having looked at the balance of production, dissipation and nonlinear transfer over the domain as a whole in §§ 4.1 & 4.2, we now consider the distribution of these terms in physical space. By doing so we identify the regions of the flow most responsible for production, dissipation and nonlinear transfer for each of the three harmonic modes.

Let us first consider the spatial distributions for DNS, which are plotted in figure 4. Each row represents a harmonic frequency (with the final row representing their aggregate) and each column represents a single physical mechanism. Although linear dissipation $\hat{D}_e(\omega)$ is generally considered as a whole, we here plot the contributions of viscous dissipation $\hat{D}(\omega)$ and energy flux out $\hat{M}(\omega)$ separately using the top and bottom halves of each panel. We note from the colour scale that, consistent with figures 2 & 3, the two dominant terms are production and dissipation for the first harmonic, $\hat{P}(\omega_1)$ and $\hat{D}_e(\omega_1)$. This is also clearly seen by comparing the production for the first harmonic with the overall production; and the dissipation for the first harmonic with the overall

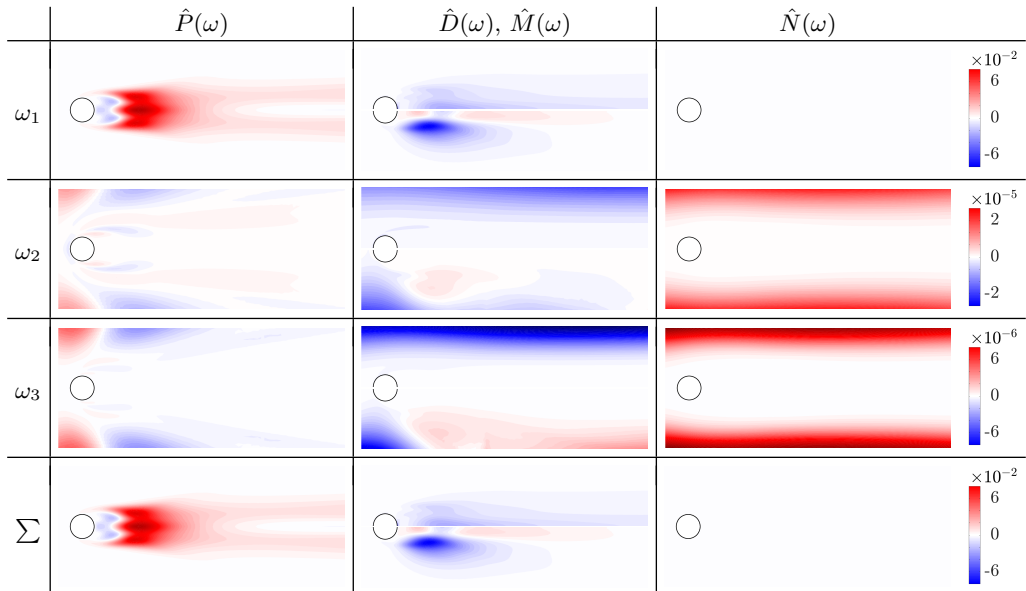


FIGURE 5. Spatial distribution of production ($\hat{P}(\omega)$), viscous dissipation ($\hat{D}(\omega)$, upper half) / energy flux out ($\hat{M}(\omega)$, lower half) and nonlinear energy transfer ($\hat{N}(\omega)$) from resolvent analysis for each harmonic frequency. Note the smaller colour scales for ω_2 and ω_3 .

dissipation. We also see that, like production and dissipation, the nonlinear transfer terms are significantly larger for the first harmonic than any other.

Let us now consider the spatial distributions for resolvent analysis, which are plotted in figure 5. We see reasonable agreement between resolvent analysis and DNS for production and dissipation for the first harmonic mode and for the flow in aggregate. The agreement for all other terms, however, is poor. Particularly striking is that the nonlinear transfer term for the first harmonic, $\hat{N}(\omega_1)$, is approximately zero at all points in physical space. This is surprising: not only is $\hat{N}(\omega_1)$ approximately zero when integrated in space (figures 2 & 3), but also at every point in space (figure 5). This implies that the inner product $\langle \hat{\mathbf{f}}_1^{(1)}, \hat{\mathbf{u}}_1^{(1)} \rangle$ is approximately zero, which is consistent with the limited spatial overlap of $\hat{\mathbf{u}}_1^{(1)}$ and $\hat{\mathbf{f}}_1^{(1)}$ in physical space and is explained by the non-normality of the resolvent operator (Symon *et al.* 2020). We can therefore say that non-normality, while facilitating linear energy transfer mechanisms, tends to hinder nonlinear energy transfer. For resolvent analysis there is approximately zero nonlinear energy transfer for the first harmonic at all points in the domain; and for the higher harmonics we observe nonlinear transfer only in the freestream.

5. Conclusions

We have investigated energy transfer mechanisms for vortex shedding behind a 2D circular cylinder at $Re = 100$. An energy balance is achieved across production, viscous dissipation and nonlinear transfer—both for the flow as a whole and for each harmonic mode. Production is generally positive and extracts energy from the mean flow, whereas viscous dissipation is always negative. Meanwhile, nonlinear mechanisms transfer energy between temporal frequencies to ensure an energy balance for each harmonic mode. Specifically, the nonlinear energy transfer is negative for the fundamental harmonic frequency ω_1 and positive for its higher harmonics. The net energy transfer across all

harmonics is zero, which implies that the nonlinear terms are conservative and that there exists an energy balance across linear mechanisms for the flow as a whole.

The energy balance achieved by the DNS was compared to that predicted by resolvent analysis. The resolvent operator, when forced at each harmonic frequency by its leading forcing mode, achieves an energy balance for each harmonic mode, and for the flow in aggregate. But it does not achieve a suitable balance for the nonlinear transfer of energy across harmonic modes. In particular the nonlinear transfer of energy from the first harmonic frequency to the second and third harmonic frequencies seen for the DNS is not captured by resolvent analysis. This helps to explain the excess energy observed in the first harmonic frequency's leading resolvent mode (figure 1 (*d*)) when compared to the true first harmonic mode shape (figure 1 (*c*)) and is explained by the non-normality of the resolvent operator. Together these observations could help in the development of better eddy-viscosity models and, more generally, better models for nonlinear energy transfer for resolvent analysis.

Declaration of Interests

The authors report no conflict of interest.

REFERENCES

- BARK, F. H. 1975 On the wave structure of the wall region of a turbulent boundary layer. *J. Fluid Mech.* **70** (2), 229–250.
- HWANG, Y. & COSSU, C. 2010 Linear non-normal energy amplification of harmonic and stochastic forcing in the turbulent channel flow. *J. Fluid Mech.* **664**, 51–73.
- ILLINGWORTH, S. J., MONTY, J. P. & MARUSIC, I. 2018 Estimating large-scale structures in wall turbulence using linear models. *J. Fluid Mech.* **842**, 146–162.
- JIANG, H. & CHENG, L. 2017 Strouhal–Reynolds number relationship for flow past a circular cylinder. *J. Fluid Mech.* **832**, 170–188.
- JIN, B., ILLINGWORTH, S. J. & SANDBERG, R. D. 2019 Feedback control of vortex shedding using a resolvent-based modelling approach. *JFM, accepted* .
- LANDAHL, M. T. 1967 A wave-guide model for turbulent shear flow. *J. Fluid Mech.* **29** (3), 441–459.
- LOGG, A., MARDAL, K. A. & WELLS, G. 2012 *Automated solution of differential equations by the finite element method: The FEniCS book*, , vol. 84. Springer Science & Business Media.
- MCKEON, B. J. & SHARMA, A. S. 2010 A critical-layer framework for turbulent pipe flow. *J. Fluid Mech.* **658**, 336–382.
- METTOT, C., SIPP, D. & BÉZARD, H. 2014 Quasi-laminar stability and sensitivity analyses for turbulent flows: prediction of low-frequency unsteadiness and passive control. *Phys. Fluids* **26** (4), 061701.
- ROSENBERG, K., SYMON, S. & MCKEON, B. J. 2019 Role of parasitic modes in nonlinear closure via the resolvent feedback loop. *Phys. Rev. Fluids* **4** (5), 052601.
- SCHMID, P. J. & HENNINGSON, D. S. 2001 *Stability and transition in shear flows*. Springer.
- SIPP, D. & MARQUET, O. 2013 Characterization of noise amplifiers with global singular modes: the case of the leading-edge flat-plate boundary layer. *Theor. Comput. Fluid Dyn.* **27** (5), 617–635.
- SYMON, S., ILLINGWORTH, S. J. & MARUSIC, I. 2020 Energy transfer in turbulent channel flows and implications for resolvent modelling. *In prep.* .
- SYMON, S., ROSENBERG, K., DAWSON, S. T. M. & MCKEON, B. J. 2018 Non-normality and classification of amplification mechanisms in stability and resolvent analysis. *Phys. Rev. Fluids* **3** (5), 053902.
- SYMON, S., SIPP, D. & MCKEON, B. J. 2019 A tale of two airfoils: resolvent-based modelling of an oscillator versus an amplifier from an experimental mean. *J. Fluid Mech.* **881**, 51–83.
- YEH, C. A. & TAIRA, K. 2019 Resolvent-analysis based design of airfoil separation control. *J. Fluid Mech.* **867**, 572–610.